PHYSICAL METALLURGY
AND HEAT TREATMENT

Effects of Hydrogen Level and Cooling Rate on Ultimate Tensile Strength of Al A319 Alloy[1]

A. Bahmani[a, b], **G. Eisaabadi B.**[c], **P. Davami**[a, b], **N. Varahram**[a, b], **and M. O. Shabani**[d, *]

[a]Razi Metallurgical Research Center, No. 8, Fernan St., Sorkhehesar Road, Km 21 Karadj Makhsous Road, Tehran—Iran
[b]Department of Materials Science & Engineering, Sharif University of Technology Tehran, Iran
[c]Department of Materials Science and Engineering, School of Engineering, University of Arak, Arak, Iran
[d]Materials and Energy Research Center (MERC), Tehran, Iran
*e-mail: vahid_ostadshabany@yahoo.com

Abstract—The present study investigated the effects of initial Hydrogen level and cooling rate on ultimate tensile strength of commercial Al-A319 alloys. Three hydrogen levels (0.01, 0.2, and 0.41 mL/100 grams of melt) and five cooling rate were studied. Total of 45 tensile test bars was prepared (three hydrogen levels × five cooling rate × three repeats). The UTS of the samples was determined though uniaxial tension tests. Furthermore, the microstructures of the samples were studied by standard metallographic technique and image analysis software. Finally the relationship between UTS and microstructurai features—SDAS and fraction of porosity (Fp%)—of the alloys was investigated.

Results of tensile test revealed: (i) UTS of the alloy decreased with increasing of hydrogen level or decreasing of cooling rate and (ii) Increasing of cooling rate beyond a certain value increased the UTS of the alloy significantly. Results of image analysis showed that the Fp% increased with increasing of hydrogen level and decreasing of cooling rate.

Finally a Matrix Index [$= -$SDAS (μm) $- 68.7$ Ln (Fp%) $+ 275$] was defined to correlate the tensile strength and microstructurai features of the alloy. It was shown that the UTS of the alloys had a linear dependence on matrix index according the below equation:

$$\text{UTS (MPa)} = 0.916 \text{ M.I} + 265.17 \quad R^2 = 0.95$$

Keywords: degassing, chilling effect, directional solidification, porosity

1. INTRODUCTION

Aluminum–silicon (Al–Si) cast alloys are becoming the most popular aluminum alloys being used in tile automotive industry mainly due to their high strength-to-weight ratio, high castability, high corrosion and wear resistance, as well as their high tensile, impact and fatigue properties after an proper heat treatment [1–6]. Many variables influence mechanical properties of Al–Si casting alloys, including [1, 3, 7–9]:

—Chemical composition of the alloy;

—Metal soundness in terms of gas and shrinkage porosity and inclusions;

—Solidification conditions (or cooling rate);

—Metallurgical characteristics including grain size, dendrite arm spacing (DAS), and the shape, size, and distribution of constituents;

—Applied heat treatment [1, 3, 7–9].

Therefore, the increased use of these alloys demands a better understanding of the effects of microstructural features and processing parameters on their mechanical properties [2].

Alloy A319 is essentially a hypoeutectic Al–Si alloy with two main solidification stages, formation of aluminum rich (Al) dendrites followed by development of two-phase Al–Si eutectic. However, the presence of additional alloying elements such as Mg and Cu, as well as of impurities such as Fe and Mn, leads to a more complex solidification sequence [2, 10].

An important defect which occurs in cast aluminum alloys is gas porosities. H (hydrogen) is the only gas that is appreciably soluble in aluminum and its alloys. Actual liquid and solid solubilities in pure aluminum just above and below the solidus are 0.69 and 0.04 ppm [11]. These values vary only slightly for most cast aluminum alloys. During cooling and solidification, H in excess of the extremely low solid solubility may precipitate in molecular form, resulting in the formation of pores. Many researchers [12–15] investigated the effect of porosities on mechanical properties of cast Al–Si alloys. It has been suggested that porosity is a leading cause in the reduction of mechanical properties, particularly elongation and fatigue resistance,

[1] The article is published in the original.

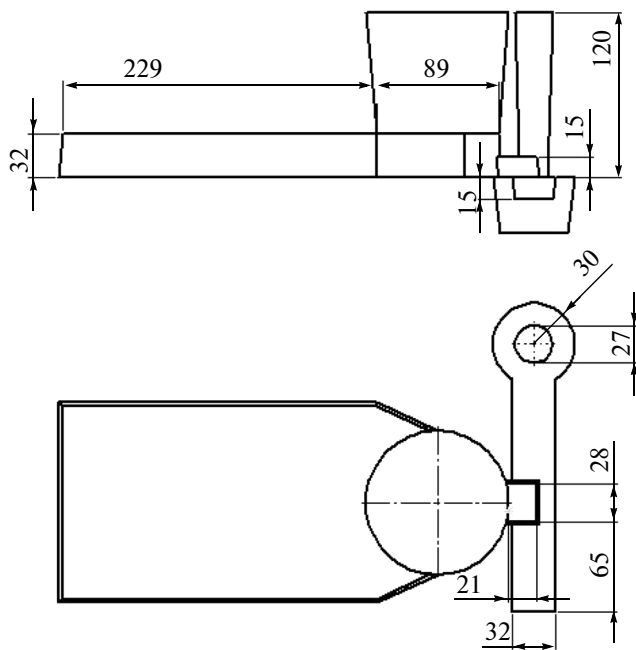**Table 1.** Chemical composition of the Al-A319 alloys used in the present study

	Al	Sb	Sn	Pb	Ni	Cr	Ti	Zn	Mg	Mn	Cu	Fe	Si
Low H castings	89.48	0.01	0.01	0.02	0.03	0.00	0.02	0.10	0.29	0.28	3.31	0.47	5.98
Medium H castings	89.49	0.00	0.01	0.01	0.01	0.00	0.02	0.01	0.25	0.28	3.07	0.45	6.37
High H castings	89.39	0.02	0.01	0.02	0.03	0.01	0.02	0.41	0.32	0.33	3.23	0.49	6.03

Table 2. Summary of investigated casting conditions

Experiment	Degassing time (minute)	Hydrogen level (mL/100 g Al)
Low hydrogen	10	0.01
Medium hydrogen	5	0.20
High hydrogen	0	0.41

as well as a loss of pressure tightness and a degradation of the surface appearance in cast parts [11]. Also, it has been reported that tensile properties of Al–Si alloys are influenced by the increasing tendency to develop porosity partly as a result of Cu [16–18] and Sr additions. Samuel et al [9] reported that the level of porosity can be kept down to a minimum by controlling the alloy chemistry and reducing the secondary dendrite arm spacing (SDAS), through fast cooling.

Increasing cooling rate during solidification not only reduces the level of porosity but also refines the silicon and Fe-rich particles and changes their shape, distributions and aspect ratio[2, 3, 8, 19]. There are more large and elongated particles in the slowly frozen microstructure than the rapidly solidified microstructure. The silicon particles thus become finer and less elongated in rapidly solidified castings. Generalfy, The size of the intermetallic particles is inversely proportional to the cooling rate (SDAS) [2]. Several researchers level [20, 21] suggested a strong linear relationship between SDAS and the average Fe platelet length, suggesting the use of SDAS as a reliable indicator of the average Fe lengths for a given Fe level. High cooling rate also hinders the precipitation of Fe and retains Fe in solid solution [22, 23]. In particular, in Al-A319 alloys solidified at relatively fast rates the negative effect of porosity on the mechanical properties can be neglected. In this case, the exhibited tensile properties of the alloy are linked to the SDAS, volume fraction, morphology and size of the intermetallic phases (including the Si precipitates), and also precipitates formed during heat treating [4, 9, 17, 24–26].

2. EXPERIMENTAL PROCEDURE

The chemical composition of the alloy that was used in present study is given in Table 1. This chemical composition corresponds to the standard Al-A319 alloy. 1000 kg of charges from the same batch of A319 was melted in an induction melting furnace at 750°C during an industrial practice in Iran Khodro Aluminum Casting Company. A rotary degasser (pure dry argon with injection rate 50 L/min at 150 rpm) was used to control the melt hydrogen level. Three levels of hydrogen were achieved through different, degassing times: 0, 5 and 10 minutes. Subsequently, the hydrogen content of the melt was analyzed by HyScan II (a product from Severn System Company) instrument. After degassing the melt was poured into a silica-bonded sand mold that is presented in Fig. 1. Table 2 represents the different casting conditions that were studied in the present study. To achieve different cooling rates, a steel chill was used at the end of mold. Three castings were poured for each level of hydrogen. After casting, the samples were machined and five tensile test bars were obtained from each casting according to ASTM B577. The distances of samples were 10, 50, 90, 130 and 170 mm from the chilled surface of the castings. Total of 45 test bars was prepared (3 samples for each distance from chill for each level of hydrogen). The test bars were pulled to fracture by an Instron 1195-5500R machine with cross-head speed of 1 mm/min. To investigate the effects of initial H content and cooling rate on the microstructure of the alloy, the microstructure of test bars was investigated by optical microscope. Using standard metallography procedure, five

Fig. 1. Geometry of mold that was used in the present study
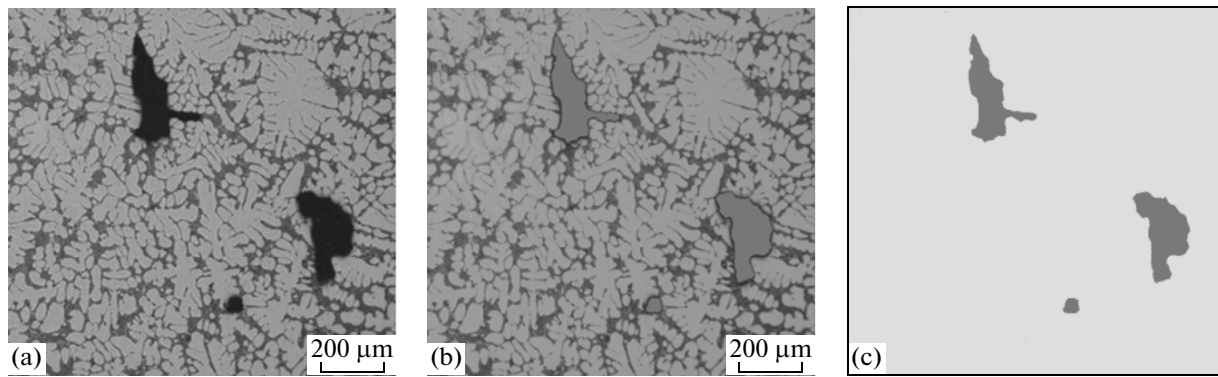
Fig. 2. Typical microstructure that was analyzed using image analysis software, (a) Original microstructure, (b) Original microstructure overlaid with binary image of pores and (c) the final binary image of (a).

metallography specimens ($10 \times 10 \times 10$ mm³) were prepared for each distance from chill and hydrogen level. Subsequently, twenty random pictures were taken from each specimen (total of 100 metallography pictures for each condition at magnification of 50×). The images were analyzed by Digimizer image analysis software (a product from MedCalc Software). From the results of image analysis, the fraction of porosity (Fp%) and secondary dendrites arm spacing (SDAS) were determined. Figure 2a shows a typical image and Figs. 2b and 2c show the Fig. 2a after processing (binarization) by image analysis software. The gray areas in Fig. 2b (red areas in Fig. 2c) are identified as pores by software.

Table 3. Tensile strength obtained for different casting conditions. The values of standard errors are shown in the bracket

Distance from chill (mm)	Low H	Medium H	High H
10	234.02[±3.41]	202.96[±6.2]	181.14[±4.51]
50	180.95[±4.51]	184.03[±5.01]	163.85[±7.1]
90	169.07[±6.12]	163.10[±3.25]	146.10[±5.9]
130	166.89[±2.89]	148.33[±2.85]	143.11[±1.56]
170	153.00[±4.13]	145.21[±3.65]	133.98[±3.79]

3. RESULTS

Table 3 shows the tensile strength obtained for each casting condition and distance from chill; the values in this table are the average of three data. Table 4 shows the results of image analysis that obtained for each experiment.

4. DISCUSSION

4.1. Relationship between Tensile Strength, SDAS and Fp%

Figures 3a, 3b and 3c show the variation of UTS, SDAS and fraction of porosity (Fp%) with distance from chilled end for three levels of dissolved hydrogen, respectively. It could be seen that in all cases, the UTS decreased with increasing the distances from chilled end. This is due to the decreasing of cooling rate with increasing the distance from chilled end. Decreasing of cooling rate increases the SDAS (Fig. 2b), coarsens the microstructure and increases length of Fe-reach phase [22] that results in decreased UTS. Furthermore, since the decreasing of cooling rate increase the available time for growth of pores it could be seen in Fig. 2c that Fp% increased with increasing the distance from chill. This increase in the Fp% decreases the load bearing surface, which results in decreased UTS (Fig. 2d), in Fig. 2a, it is interesting to notice that increasing of cooling rate in the first three samples (from a to c) did not changed the UTS signif-
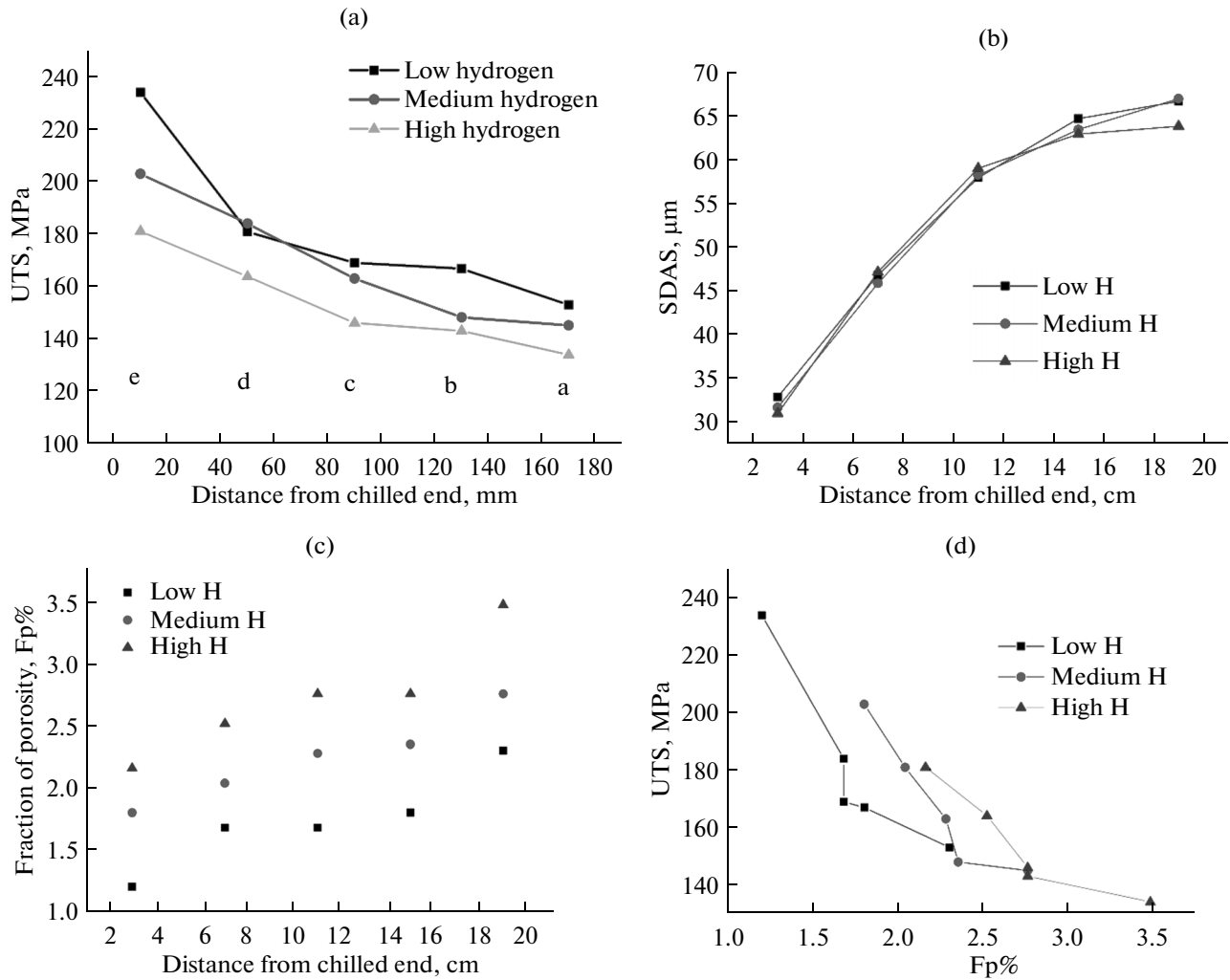
Table 4. Results of image analysis obtained for each experiment. SDAS (μm) and Fp (%)

Distance from chill (mm)	Low H		Medium H		High H	
	SDAS	Fp	SDAS	Fp	SDAS	Fp
10	32.70	1.20	31.50	1.80	30.80	2.16
50	46.75	1.68	45.80	2.04	47.10	2.52
90	57.96	1.70	58.25	2.28	59.03	2.76
130	64.75	1.80	63.50	2.35	62.98	2.85
170	66.75	2.30	67.05	2.76	63.89	3.48

(a)

(b)

(c)

(d)

Fig. 3. Variation of UTS with distance from mold end for (a) end chilled and (b) not-chilled

icantly. But on the other hand increasing cooling rate from c to e increased the UTS significantly. Therefore, it seems that increasing of cooling rate beyond a certain values will results in significantly large UTS valuep in examined alloy.

From Fig. 3a, it could be seen that UTS decreased with increasing of the hydrogen level. It could be explained through the increasing of Fp% with increasing the hydrogen level (Fig. 3c). In samples that experienced a perfect degassing (i.e. low hydrogen castings with hydrogen level of 0.01 mL/100 g Al) the available hydrogen for nucleation of gas pores was decreased effectively and therefore the chance for their nucleation decreased to large extent. On the other hand, increasing of hydrogen level increased the available hydrogen for nucleation of porosities. Although, several researchers [4, 9, 17, 24−26] reported that the fast solidification rates eliminates the negative effect of porosity on the mechanical properties of Al−Si cast-

ings, it could be seen that even the very high cooling rate (in samples with 10 mm distance from chilled end) the UTS showed a considerable decrease with increasing the dissolved hydrogen level. Therefore, the fast solidification rate did not eliminate the negative effect of hydrogen.

4.2. Prediction of Tensile Strength

The data obtained from the study of microstructure (SDAS and Fp%) and results of tensile test was used for prediction of tensile strength as a function of microstructural features. Finally a matrix index was defined as Eq. 1. The matrix index was defined in such a way that represents the effects of both solidification rate (SDAS) and fraction of porosity (Fp%).

$$\text{Matrix Index} = -\text{SDAS}(\mu m) - 68.7\text{Ln}(\text{Fp\%}) + 275. \quad (1)$$

Figure 4 shows the variation of tensile strength with matrix index of the examined samples. From this fig-
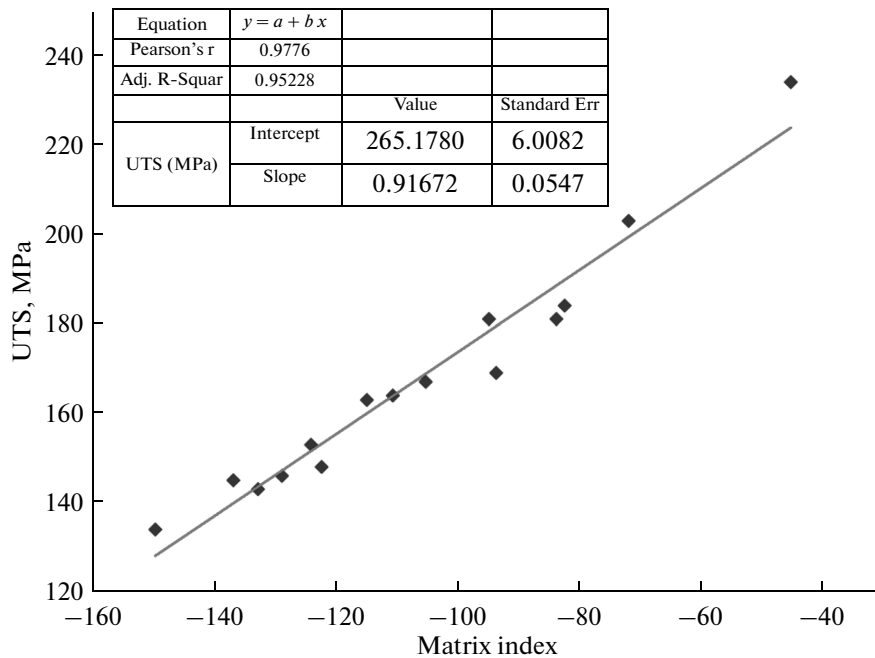
Equation	$y = a + b\,x$		
Pearson's r	0.9776		
Adj. R-Squar	0.95228		
		Value	Standard Err
UTS (MPa)	Intercept	265.1780	6.0082
	Slope	0.91672	0.0547

Fig. 4. Variation of tensile strength with matrix index that was defined in Eq. 1.

ure it could be seen that there was a clear linear relationship between the measured UTS values and matrix index of the samples. Since the adjust R-square of fitted line is 0.95 this relationship could be used for prediction of tensile strength in examined alloy. Therefore, according to Fig. 4, the UTS of the alloys varied with variation of matrix index according to Eq. 2

$$\text{UTS(MPa)} = 0.916 M.1 + 265.17 \quad R^2 = 0.95 \quad (2)$$

5. CONCLUSIONS

—The tensile strength of the alloys decreased with increasing the hydrogen content of the melt. But it should be noted that the scattering of tensile strength decreased with increasing the hydrogen content of the melt.

—It was shown that despite many other researches, increasing of cooling rate did not eliminate the negative effects of high hydrogen level, even in samples that was very close to the chilled end of the castings.

—Increasing of cooling rate resulted in higher tensile strength in all hydrogen level.

—It was shown that the tensile strength of the examined alloy could be predicted using the proposed matrix index.

REFERENCES

1. Sebaie, O.E., Samuel, A., Samuel, F., and Doty, H., *Mater. Sci. Eng.*, 2008, vol. A 480, pp. 342–355.

2. García-Garcia, G., Espinoza-Cuadra, J., and Mancha-Molinar, H., *Mater. Des.*, 2007, vol. 28, pp. 428–433.

3. Firouzdor, V., Rajabi, M., Nejati, E., and Khomamizadeh, F., *Mater. Sci. Eng.*, 2007, vol. A 454, pp. 528–535.

4. Rincon, E., Lopez, H., Cisneros, M., and Mancha, H., *Mater. Sci. Eng.*, 2009, vol. A 519, pp. 128–140.

5. Eisaabadi, G.B., Davami, P, Kim, S., and Varahram, N., *Mater. Sci. Eng.*, 2012, vol. A 552, pp. 36–47.

6. Eisaabadi, G.B., Varahram, N., Davami, P., and Kim, S.K., *Mater. Sci. Eng.*, 2012, vol. A 548, pp. 99–105.

7. Kashyap, K., Murali, S., Raman, K., and Murthy, K., *Mater. Sci. Technol.*, 1993, vol. 9, pp. 189–204.

8. Sigworth, G., Shivkumar, S., and Apelian, D., *Trans. AFS*, 1989, vol. 97, pp. 811–824.

9. Samuel, A. and Samuel, F., *Metall. Mater. Trans.,* 1995, vol. A 26, pp. 2359–2372.

10. Martinez, E.D., Cisneros, M.G., Valtierra, S., and Lacaze, J., *Scr. Mater.*, 2005, vol. 52, pp. 439–443.

11. Anson, J. and Gruzleski, J., *Mater. Charact.*, 1999, vol. 43, pp. 319–335.

12. Ma, Z., Samuel, A., Samuel, F., Doty, H., and Valtierra, S., *Mater. Sci. Eng.*, 2008, vol. A 490, pp. 36–51.

13. Tekmen, C., Ozdemir, I., Cocen, U., and Onel, K., *Mater. Sci. Eng.*, 2003, vol. A 360, pp. 365–371.

14. Irfan, M., Schwam, D., Karve, A., and Ryder, R., *Mater. Sci. Eng.*, 2011, vol. A 535, pp. 108–114.

15. Dispinar, D., Akhtar, S., Nordmark, A., and Syvertsen, F., *Adv. Mater. Res.*, 2012, vol. 445, pp. 283–288.

16. Caceres, C., Djurdjevic, M., Stockwell, T., and Sokolowski, J., *Scr. Mater.*, 1999, vol. 42.

17. Li, Z., Samuel, A., Samuel, F., Ravindran, C., and Valtierra, S., *Mater. Sci. Eng.*, 2004, vol. A 367, pp. 96–110.

18. Heiberg, G., Raanes, M., Arnberg, L., Nogita, K., Dahle, A., and Dons, A., *Trans. AFS*, 2002, vol. 110, pp. 347–358.

19. Bahmani, A., Hatami, N., Varahram, N., Davami, P., and Shabani, M.O., *Int. J. Adv. Manuf. Technol.*, 2012, vol. 64, pp. 1313–1321.

20. Pennors, A., Samuel, A., Samuel, F., and Doty, H., *Trans. AFS*, 1998, vol. 106, pp. 251–264.

21. Samuel, A., Pennors, A., Villeneuve, C., Samuel, F., and Doty, H., *Int. J. Cast Met. Res.,* 2000, vol. 13, p. 231.

22. Cao, X. and Campbell, J., *Mater. Trans., JIM,* 2006, vol. 47, pp. 1303–1312.

23. Shabani, M.O., Mazahery, A., Bahmani, A., Davami, P., and Varahram, N., *Kovove Mater.*, 2011, vol. 49, pp. 253–264.

24. Hafiz, M.F. and Kobayashi, T., *Scr. Metall. Mater.*, 1994, vol. 30.

25. Saigal, A. and Fuller, E.R., *Computational Materials Science*, 2001, vol. 21, pp. 149–158.

26. Samuel, F., Samuel, A., and Doty, H., *Trans. AFS,* 1996, vol. 104, pp. 893–902.